NUCL SCI TECH (2019) 30:120
https://doi.org/10.1007/s41365-019-0649-4

Experimental validation of material discrimination ability of muon scattering tomography at the TUMUTY facility

Xing-Yu Pan[1] · Yi-Fan Zheng[2,3] · Zhi Zeng[1] · Xue-Wu Wang[1] · Jian-Ping Cheng[4]

Received: 22 February 2019 / Revised: 22 February 2019 / Accepted: 11 April 2019 / Published online: 11 July 2019

Abstract Muon scattering tomography is believed to be a promising technique for cargo container inspection, owing to the ability of natural muons to penetrate into dense materials and the absence of artificial radiation. In this work, the material discrimination ability of muon scattering tomography is evaluated based on experiments at the Tsinghua University cosmic ray muon tomography facility, with four materials: flour (as drugs substitute), aluminum, steel, and lead. The features of the different materials could be discriminated with cluster analysis and classifiers based on support vector machine. The overall discrimination precisions for these four materials could reach 70, 95, and 99% with 1-, 5-, and 10-min-long measurement, respectively.

Keywords Muon tomography · Cargo container inspection · Material discrimination · SVM classifier

✉ Zhi Zeng
zengzhi@tsinghua.edu.cn

1 Key Laboratory of Particle and Radiation Imaging (Ministry of Education) and Department of Engineering Physics, Tsinghua University, Beijing 100084, China

2 Department of Nuclear Engineering, University of California, Berkeley, CA 94709, USA

3 Department of Radiology and Biomedical Imaging, University of California, San Francisco, CA 94143, USA

4 College of Nuclear Science and Technology, Beijing Normal University, Beijing 100875, China

1 Introduction

Cosmic rays, mainly originating from outside the solar system, produce showers of secondary particles, which are able to reach the sea level. At the Earth's surface, muons are the most numerous charged particles and have an intensity of approximately 1 $\mathrm{cm}^{-2}\ \mathrm{min}^{-1}$ [1]. The muon scattering tomography technique [2], which exploits the multiple Coulomb scattering of muons, has been applied in various fields, including cargo container inspection [3–6] and spent nuclear fuel monitoring [7, 8]. This technique shows potential advantages owing to the ability of natural muons to penetrate dense materials and the absence of artificial radiation.

Previous studies have shown that muon scattering tomography is more sensitive to high-*Z* materials, including uranium, tungsten, and lead. The performance of this technique with light materials is limited by the deep penetration of muons. However, during cargo container inspection, attention should be paid to both high-*Z* materials and light materials, such as drugs and explosives. If the identification ability of muon scattering tomography for light materials could be improved, it would play a more important role in cargo container inspection.

In our previous work, we proposed the application of machine learning to identify drugs and explosives based on simulated datasets [9]. Evidence shows that the statistical results of the scattering densities of different materials are distinguishable. To perform material classification utilizing statistical results, a machine learning method based on support vector machine (SVM) was applied. In machine learning, SVMs are supervised learning models that analyze data for classification and regression analysis. The basic idea is trying to divide examples into different categories by a gap as wide as possible, which agrees with the problem of material classification. The SVM method is fully capable of performing materials identification if the features of different materials are derived. According to our previous simulation, drugs and explosives can be discriminated from air and metals with acceptable measurement durations using SVM classifiers. However, the spatial resolution of the detector was ignored and the simulated classifier did not distinguish the actual materials perfectly. In this work, a series of experiments were designed and conducted at the TUMUTY facility to validate the material discrimination ability of muon scattering tomography with four different materials [10].

2 Methodology

2.1 Principle

Muon scattering tomography utilizes the multiple Coulomb scattering interactions between muons and materials. Muons traversing a medium could be deflected by many small-angle scatters. The net 2D scattering angles approximately follow a Gaussian distribution with zero mean and variance, given by [1]:

$$\sigma_\theta \cong \frac{13.6\,\mathrm{MeV}}{\beta c \boldsymbol{p}} \sqrt{X/X_0}, \tag{1}$$

where c is the speed of light, β is the ratio of the muons' speed to the speed of light, $\boldsymbol{p}$ is the muons' momentum, X is the thickness of the medium, and X_0 is the radiation length, which can be described by [1]:

$$X_0 \cong \frac{A \cdot 716.4\,\mathrm{g/cm^2}}{\rho \cdot Z(Z+1)\ln\left(287/\sqrt{Z}\right)}, \tag{2}$$

where A is the atomic mass, Z is the atomic number, and ρ is the density. It can be seen that the variance of the scattering angles is dependent on the properties of the materials for muons with the same energies. Generally, materials with higher densities and larger atomic numbers always give larger scattering angle variances. Based on Eq. (1), the scattering density, which is dependent on the radiation length and muon momentum, can be defined as:

$$\lambda(p, X_0) = \sigma_\theta^2/X \cong \left(\frac{13.6\,\mathrm{MeV}}{p}\right)^2 \frac{1}{X_0}, \tag{3}$$

where λ represents the scattering density and has units of rad^2/cm. The approximation $\beta c \cong 1$ for muons is used in this equation. Thus, the properties of the target materials could be found, if precise scattering densities are given. A number of algorithms have been developed to reconstruct the scattering densities, including the PoCA, MLSD, and MAP [11, 12]. Among all the algorithms, the PoCA algorithm is the one with the lower computation and memory usage, and it performs well with short measurement durations.

However, it should be noted that the energy of natural muons is not constant, which leads non-constant scattering densities for certain materials. The statistical fluctuation of reconstructed scattering densities is the main factor limiting the material discrimination ability, especially for low-Z materials. To decrease the effect of the statistical fluctuation, a discrimination method based on cluster analysis has been developed. The basic assumption of this method is that materials in neighbor voxels are very likely to be the same. Because containers are filled with the same materials during transportation and given that the voxels in this work have a size of 1 cm, which is much lower than the size of cargoes, it is reasonable to assume that voxels within a certain region (for example, a region of $20 \times 20 \times 20$ cm^3) are the same. By combining all the reconstructed scattering densities in the region, it is very likely that the effects of the statistical fluctuation are reduced. Our previous simulation has confirmed that the mean value and standard deviation of the scattering densities in a region can be utilized as features to perform materials discrimination [9].

2.2 Experiment setup

To evaluate the material discrimination ability of muon scattering tomography, a series of experiments were designed and conducted at the TUMUTY facility (Fig. 1). The facility consists of six layers of large-scale position-sensitive MRPC detectors, forming an efficient detection area with a size of $70 \times 70 \times 70$ cm^3. The detectors show a good spatial resolution of approximately 0.6 mm. However, the detection efficiency of each detector is approximately 80% at present and the total efficiency of the system is only approximately 26%.

Three experiments with different designs were carried out with four different materials: flour, aluminum, steel, and lead (Fig. 2). Flour was chosen as the substitute of drugs, which are materials of great concerns for cargo container inspection. Flour was placed in a $20 \times 20 \times 20$ cm^3 cubic plastic box. Aluminum, steel, and lead were selected to represent low-Z, medium-Z, and high-Z metals, respectively.

The first experiment was designed to simulate a container of different cubic materials. The flour box and a $20 \times 20 \times 20$ cm^3 cubic aluminum box were placed side by side with a central distance of approximately 30 cm. Two lead bricks were stacked together, forming a $20 \times 10 \times 10$ cm^3 lead box. The three materials were placed on a platform in the middle of the TUMUTY

Fig. 1 Photograph of TUMUTY

facility. For the first experiment, measurements were taken over 10 days.

The second experiment was carried out to show the discrimination ability for hidden materials. The flour box was surrounded by several steel cylinders to simulate a situation in which a low-Z non-metallic material is hidden inside medium-Z metals. The size of each steel cylinder was 10 cm in diameter and 20 cm in height. For the second experiment, measurements were taken over 5 days.

The third experiment was similar to the second experiment in some aspects. The flour box was placed in the middle of a hollow steel box with a length of 40 cm, a height of 5 cm, and a thickness of 2 cm. For the third experiment, measurements were taken over 4 days.

3 Results and discussion

3.1 Image reconstruction

In this work, the PoCA algorithm was applied to reconstruct the scattering densities of spatial voxels. Sometimes a false triggering of a single detector may occur, which result in wrong muon tracks, leading to poor results. To avoid this, the trajectories of muons were fitted with the principle component analysis (PCA) method before reconstruction and the trajectories with poor linearity were rejected.

It should be noted that the effective measuring time is not equal to the actual data collection time because of the detector efficiency and trajectory selection. The effective time can be calculated from the number of muons impinging on the detection area. A Monte Carlo simulation based on the actual geometry of the TUMUTY using the Geant4 toolkit was performed to calculate the muon acceptance of the system. Considering that the muon flux at sea level is approximately 1 cm^{-2} min^{-1}, the simulation showed that approximately 1600 muons per min impinged on the detection area. During the first experiment, 433560 valid trajectories were collected after data cutoff, and the equivalent time was approximately 270 min. The equivalent times of experiments 2 and 3 were 220 and 50 min, respectively. The detection efficiency of the system was ignored temporarily because we wanted to investigate the inherent material discrimination ability of the muon scattering tomography system.

The scattering densities in the three experiments were reconstructed using the PoCA algorithm. The size of the voxels was set to $1 \times 1 \times 1$ cm^3. The densities of each experiment were summed together along the Z- and Y-axes, as shown in Fig. 3, for a more effective demonstration. The regions of different materials were marked with rectangles in X–Y projection images. The color bars in Fig. 3 represent the absolute values of the scattering densities. The shapes and sizes of lead and steel materials can be clearly identified in the projection images of all the experiments. The signal from the aluminum box in experiment 1 is low but still distinguishable. However, the scattering densities of the flour box in all the experiments are similar to that of the background, whose material is air. The inherent scattering density of flour is significantly low due to its small atomic number and low density. Thus, the statistical fluctuations caused by the detectors' spatial resolution and PoCA algorithm make it more difficult to distinguish flour from the background.

To evaluate the performance of the short time scanning, the datasets from the first 10 min of all the experiments were reconstructed separately, as shown in Fig. 4. In this situation, slight differences can be observed in the region of dense materials. However, it is still difficult to distinguish different materials, because of large fluctuations caused by the small quantity of incident muons. For datasets from shorter measuring times, the results of different materials are more difficult to be distinguished.

3.2 Material discrimination ability

To evaluate the statistic features of different materials with short measuring times, the dataset of each experiment was divided into subsets with results taken over 1, 5, and 10 min. For example, the dataset of experiment 1 can be divided into 270 subsets of 1-min measurements, 54 subsets of 5-min measurements, and 27 subsets of 10-min

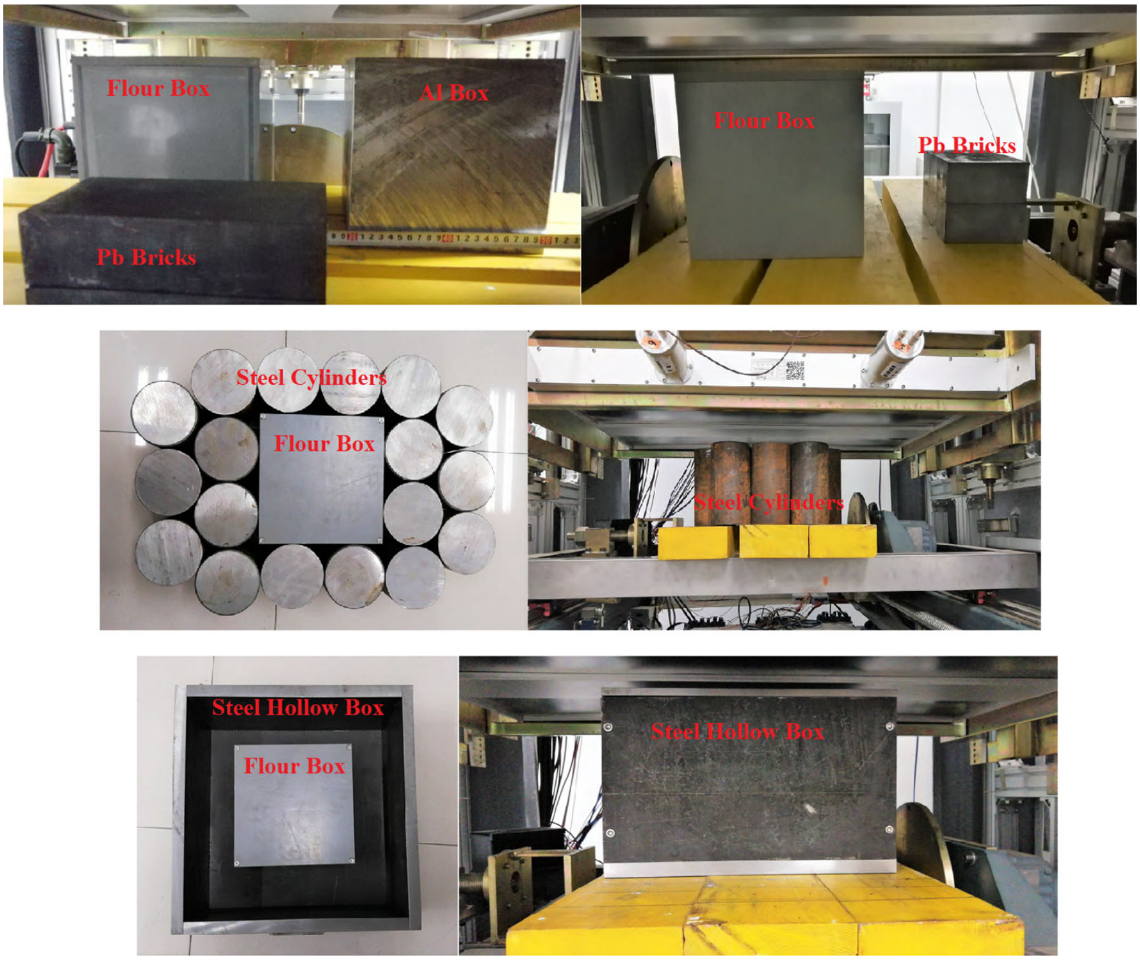

Fig. 2 The geometry layouts of the three experiments. The top part is layout of experiment # 1 (left *X–Z* view; right *Y–Z* view), the middle part is layout of experiment #2 (left *X–Y* view; right *Y–Z* view), and the bottom part is layout of experiment #3 (left *X–Y* view; right *Y–Z* view)

measurements. Each subset can be treated as an individual measurement. The following analysis is based on the subsets.

Some regions were selected as regions of interest (ROIs) for further analysis depending on the actual positions of the materials, as shown in Fig. 3. Two cubic regions were selected for the steel cylinders in experiment 2 within the side of the flour box, marked with red rectangles in Fig. 3b. Besides the measured materials, regions of the background were selected as well to represent the results from air, marked with blue rectangles in Fig. 3.

3.2.1 Discrimination of materials from the background

Owing to the PoCA algorithm principle, when the quantity of muons is not large enough, which is common for short measuring times, the reconstructed density of many voxels is zero, because no PoCA points arise in these voxels. For voxels with high atomic numbers, there is a higher probability that PoCA points are reconstructed inside these voxels. The percentages of nonzero voxels in different material regions were calculated based on subsets with different measuring times, as shown in Fig. 5.

The percentages of nonzero voxels are expected to follow a normal distribution based on the central limit theorem, fitted in Fig. 5. It can be seen that the percentages for the same material with different measuring times are nearly proportional to the measuring times. Furthermore, the denser is the material, the smaller is the percentage of nonzero voxels. The percentage of air is clearly lower than that of other materials. However, the difference between other materials is not so obvious, especially between flour and aluminum. Thus, air can be effectively distinguished from other materials. Among all the materials, flour has the biggest effect on air identification because of its low atomic number. The overlap probability of air and flour can be obtained using fitted normal distributions, which is approximately 2.31% for 1-min datasets. For 5- and 10-min datasets, the false probability is lower than 0.01%, which can be ignored. Moreover, the percentages of nonzero

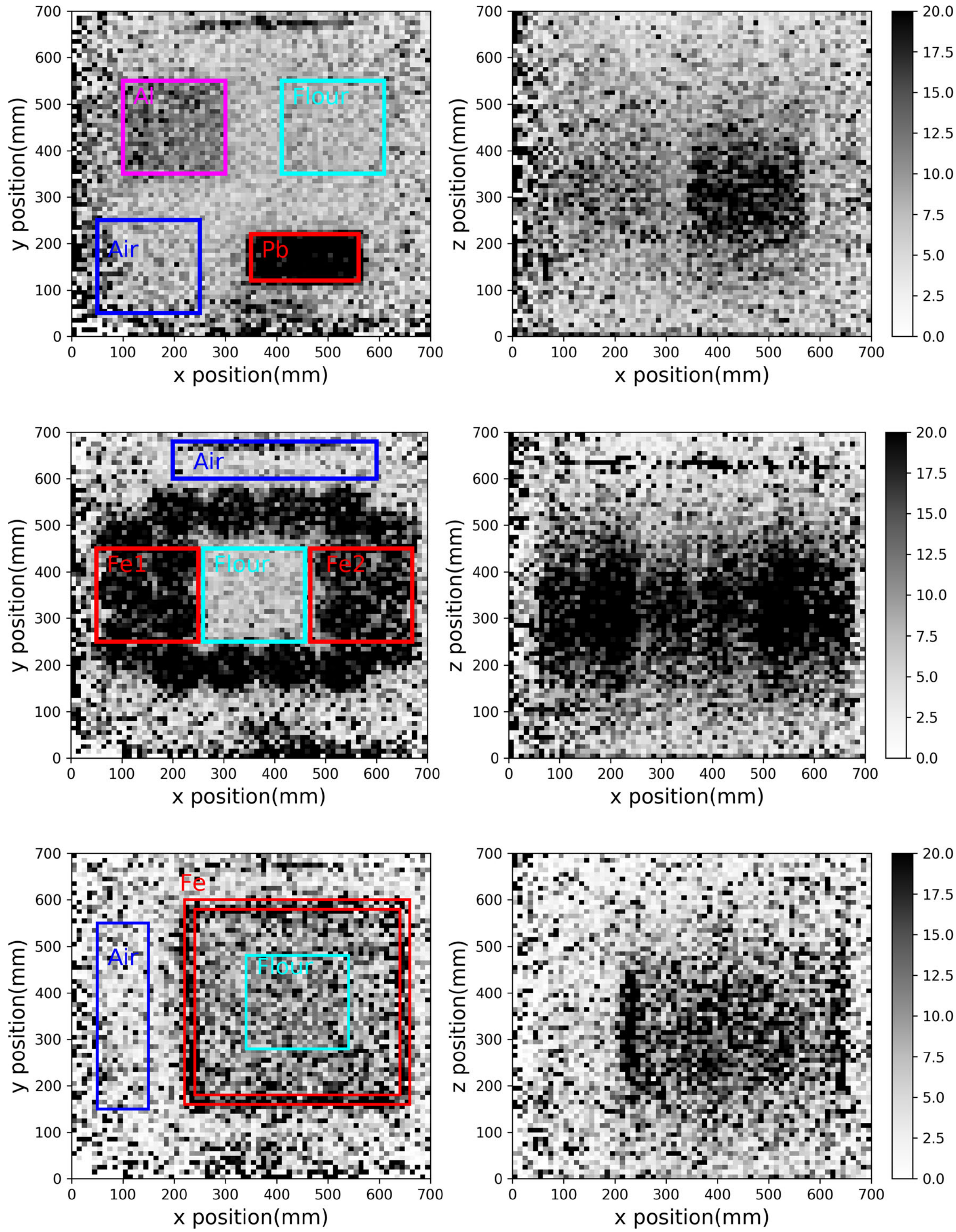

Fig. 3 The reconstructed results of the three experiments with the full dataset (from top to bottom: results are derived from experiment #1, #2, #3, respectively). The images on the left are projection images on the *X*–*Y* plane, and those in the right are projection images on the *X*–*Z* plane

voxels are significantly low for all the materials. Even for dense materials, such as Fe, the value is only 0.5% per min, leading to the poor discrimination ability using the scattering density for short time measurement, as shown in Fig. 4.

3.2.2 Materials discrimination

To analyze the differences between the measured materials, the reconstructed scattering densities in ROIs with different materials were extracted; the distributions

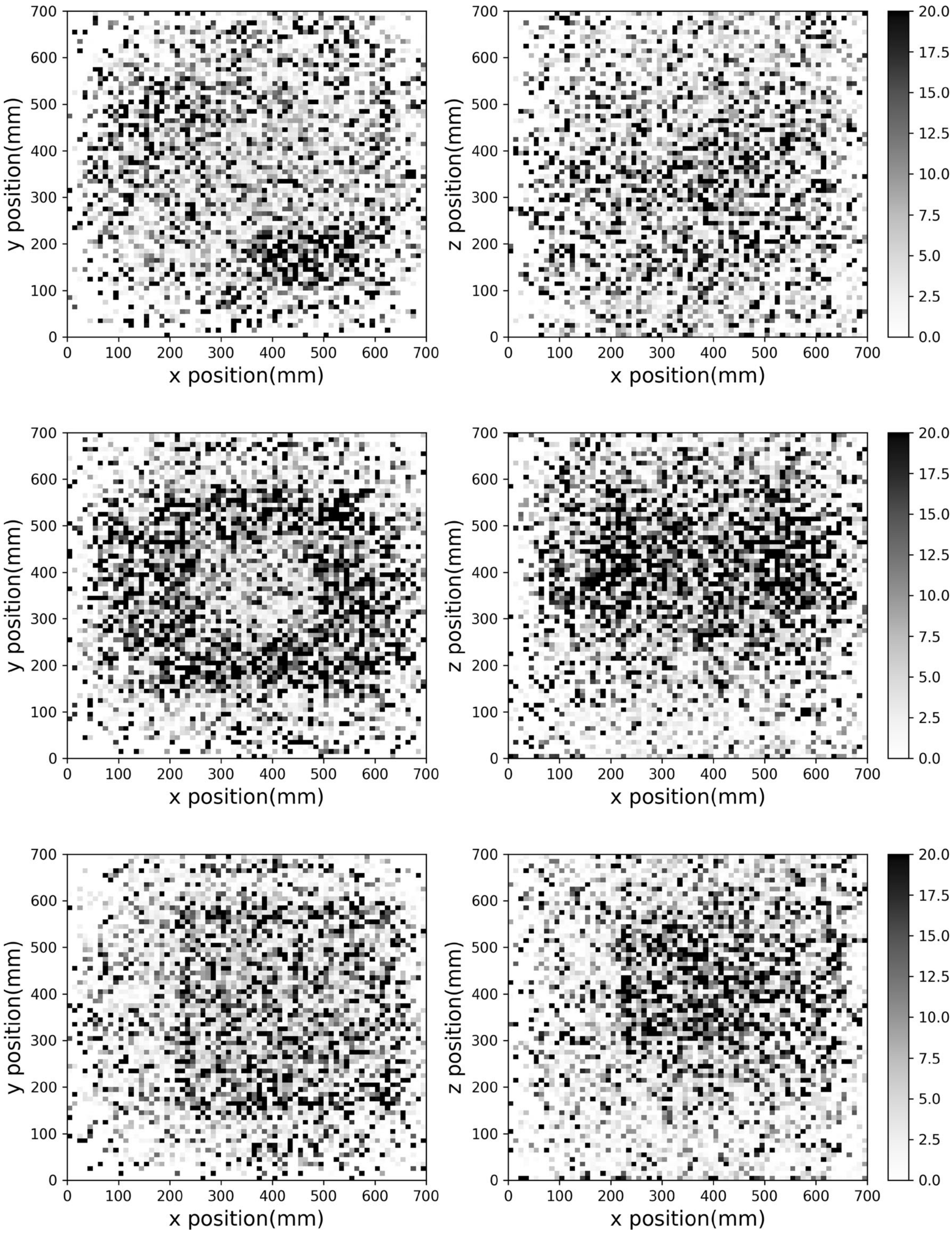

Fig. 4 The reconstructed results of the three experiments with 10-min datasets (from top to bottom: results are derived from experiment #1, #2, #3, respectively). The images on the left are projection images on the *X*–*Y* plane, and those on the right are projection images on the *X*–*Z* plane

are shown in Fig. 6. The values of air, flour, aluminum, and lead come from experiment 1, and the values of steel come from experiment 2. It can be seen that even in the region of low-*Z* material, large scattering densities are obtained. The deviations of the scattering densities for all the materials are large compared to the mean values, which makes it difficult to identify the material in a single voxel. However, the difference in the distributions of the scattering densities for the materials is still present. Obviously, the mean values and standard deviations for dense materials are larger

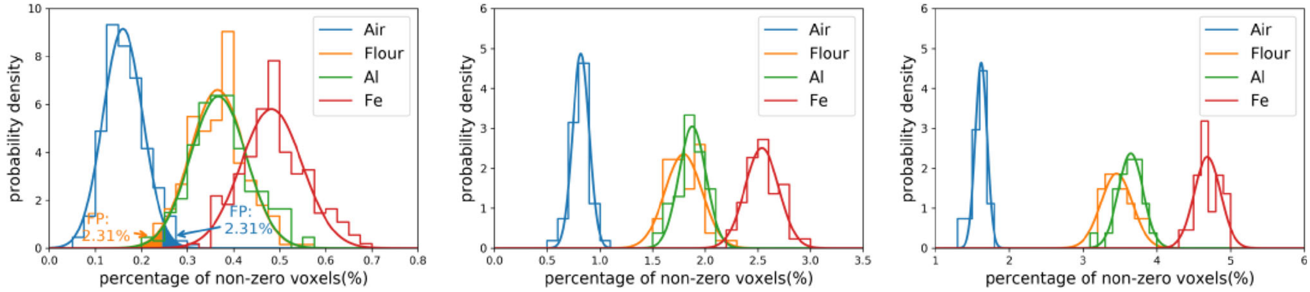

Fig. 5 (Color online) The distribution of percentages of nonzero voxels from regions with different materials (from left to right: the equivalent times are 1, 5, and 10 min, respectively)

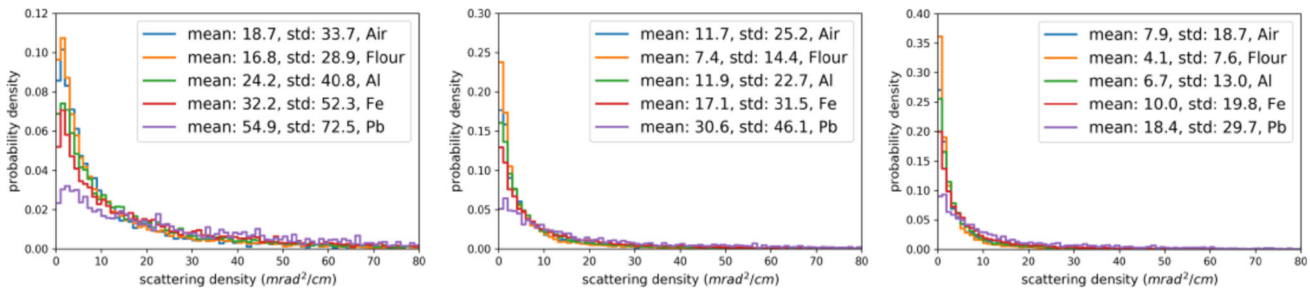

Fig. 6 (Color online) The distribution of the scattering densities from regions with different materials (from left to right: the equivalent times are 1, 5, and 10 min, respectively)

than those for low-*Z* materials. Although it is difficult to discriminate a material from a single voxel, it is still possible to perform discrimination in a region of the same materials with multiple voxels according to the distribution of the scattering densities. The mean value and standard deviation are two of the most important features for the distribution, which could be used as features for material discrimination.

The mean values and standard deviations of the scattering densities in all ROIs of the three experiments were calculated, as shown in Fig. 7. Each data point represents the mean value and standard deviation of the scattering densities in a certain ROI, obtained using sub-datasets with different measuring times. A difference between all materials is visible, especially for the 10-min dataset. With a 10-min measurement, the four materials (flour, aluminum, steel, and lead) could be clearly distinguished. For 1- and 5-min measurements, the difference is not as clear but it provides a possible method to perform material discrimination. However, the result of air is not as satisfying because it overlaps with the results of flour and aluminum, even with 10-min measurements. Nevertheless, this is not particularly important because the discrimination between air and other materials can be achieved by the percentage of nonzero voxels, as previously described.

The comparison of the results of the sub-datasets from different measuring times shows that different mean values and standard deviations from the same material are not the same. For example, the mean values of lead are distributed around 60 mrad^2/cm in 1-min measurements, but those in the 5- and 10-min sub-datasets are 30 and 20 mrad^2/cm, respectively. A decrease in the standard deviations with

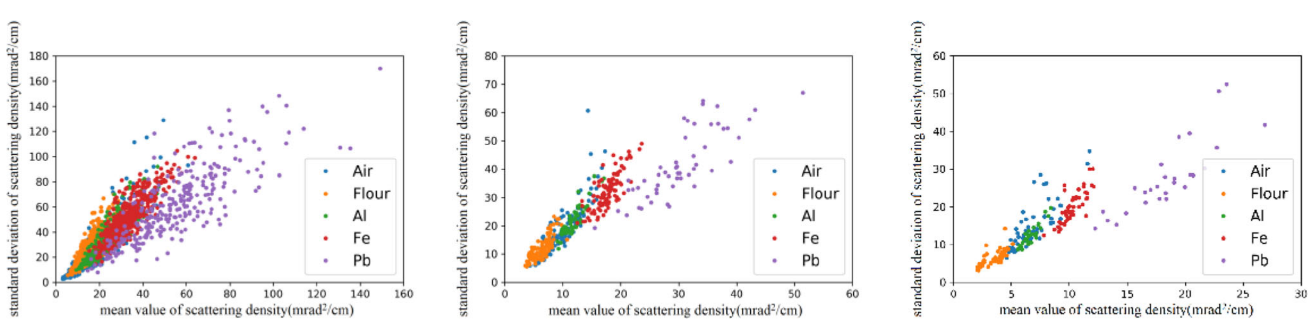

Fig. 7 (Color online) The mean values and standard deviations of the scattering densities in regions with different materials (from left to right: the equivalent times is 1, 5, and 10 min, respectively)

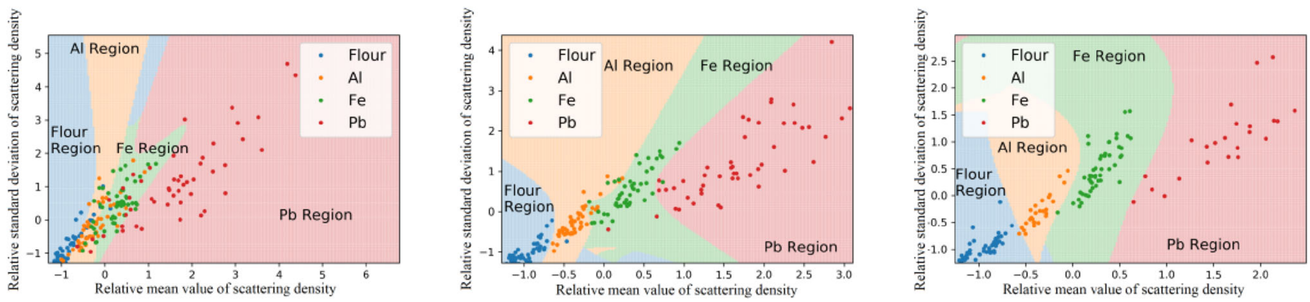

Fig. 8 (Color online) SVM classifiers of different materials (from left to right: the equivalent time is 1, 5, and 10 min, respectively)

Table 1 Discrimination precisions of different materials obtained using the SVM classifiers

Measuring time (min)	Discrimination precision				
	Flour (%)	Al (%)	Fe (%)	Pb (%)	Total (%)
1	75	50	73	76	70
5	96	100	94	89	95
10	100	93	100	100	99

increasing measuring time was also observed. The same problem occurred in the previous simulation [9]. The simulated results show that the decreasing tendency will become less pronounced, i.e., they will become more stable, for measuring times longer than 20 min. This may be because of the limitation of the PoCA algorithm. When the size of the dataset is not large enough, the statistical fluctuations of the reconstructed scattering densities are very large. Despite the inconsistency of the results with different measuring times, the results for different materials with the same measuring time seem to be relatively stable. Thus, different material discrimination models could be trained according to the measuring time.

The mean values and standard deviations of the scattering densities could be used as two features for further training of the classifiers. In this study, SVM-based classifiers were used because of their good performance for classified separation. Before training the SVM models, the features were normalized by:

$$x' = \frac{x - \bar{x}}{\sigma}, \tag{4}$$

where x represents the raw value of the feature, $\bar{x}$ represents its mean value, σ represents its standard deviation, and x' represents the normalized value of the feature. Normalization is a common preprocessing method in the field of machine learning.

In this study, only half of the datasets were used to train the SVM classifiers and the other half were used as test datasets to evaluate the performance of the classification. Due to the inconsistency of features with different measuring times, different models were trained for 1-, 5-, and 10-min sub-datasets, as shown in Fig. 8. The region in Fig. 8 was subdivided into four regions with different colors, representing the results of the SVM classification. The data points were actual results derived from sub-datasets of the three experiments. The performance of the classifiers was evaluated with test datasets; the detailed precisions of different materials are listed in Table 1. The overall precisions of the four materials for 1-, 5-, and 10-min measurements are 70, 95, and 99%, respectively. It could be concluded that the longer is the measuring time, the more precise is the classification. Even when the measuring time is only 1 min, the precisions for most materials are higher than 70%, which is acceptable for short time measurements. With this method, material discrimination with muon scattering within short measuring times was achieved.

4 Conclusion

In this work, we evaluated the material discrimination ability of muon scattering tomography with short measuring times in experiments at the TUMUTY facility. In these experiments, flour, aluminum, steel, and lead were chosen to represent materials with atomic numbers ranging from low to high. To reduce the statistical fluctuations within short measurements, a strategy based on cluster analysis was utilized. The percentage of the reconstructed nonzero scattering density could be used to discriminate materials from the background with an error rate of 2.31% for 1-min measurement. The mean value and standard deviation of the scattering densities were utilized to perform material discrimination. With SVM classifiers, the overall classification precisions for these four materials from 1-, 5-, and 10-min measurements are 70, 95, and 99%, respectively.

However, the detection efficiency was ignored because we wanted to investigate the inherent discrimination ability of muon scattering tomography. If the efficiency is considered, poor results will be achieved due to the poor efficiency of the TUMUTY. However, this problem can be solved by using a facility with higher detection efficiency. Another limitation of this method is that the results obtained with different measuring times are not consistent. Overcoming this limitation requires further research.

References

1. K.A. Olive, K. Agashe, C. Amsler et al., Review of particle physics. Chin. Phys. C **38**, 090001 (2014). https://doi.org/10.1103/PhysRevD.98.030001
2. S. Procureur, Muon imaging: principles, technologies and applications. Nucl. Instrum. Methods A **878**, 169–179 (2017). https://doi.org/10.1016/j.nima.2017.08.004
3. V. Antonuccio, M. Bandieramonte, D.L. Bonanno et al., The muon portal project: design and construction of a scanning portal based on muon tomography. Nucl. Instrum. Methods A **845**, 322–325 (2017). https://doi.org/10.1016/j.nima.2016.05.006
4. G. Blanpied, S. Kumar, D. Dorroh et al., Material discrimination using scattering and stopping of cosmic ray muons and electrons: differentiating heavier from lighter metals as well as low-atomic weight materials. Nucl. Instrum. Methods A **784**, 352–358 (2015). https://doi.org/10.1016/j.nima.2014.11.027
5. P. Baesso, D. Cussans, C. Thomay et al., Toward a RPC-based muon tomography system for cargo containers. J. Instrum. **9**, C10041 (2014). https://doi.org/10.1088/1748-0221/9/10/C10041
6. L. Frazão, J. Velthuis, C. Thomay et al., Discrimination of high-z materials in concrete-filled containers using muon scattering tomography. J. Instrum. **11**, P07020 (2016). https://doi.org/10.1088/1748-0221/11/07/P07020
7. D. Poulson, J.M. Durham, E. Guardincerri et al., Cosmic ray muon computed tomography of spent nuclear fuel in dry storage casks. Nucl. Instrum. Methods A **842**, 48–53 (2017). https://doi.org/10.1016/j.nima.2016.10.040
8. J.M. Durham, D. Poulson, J. Bacon et al., Verification of spent nuclear fuel in sealed dry storage casks via measurements of cosmic-ray muon scattering. Phys. Rev. Appl. **9**, 44013 (2018). https://doi.org/10.1103/PhysRevApplied.9.044013
9. Y. Zheng, Z. Zeng, M. Zeng et al., Discrimination of drugs and explosives in cargo inspections by applying machine learning in muon tomography. High Power Laser Part. Beams **30**, 086002 (2018). https://doi.org/10.11884/HPLPB201830.180062
10. X. Wang, M. Zeng, Z. Zeng et al., The cosmic ray muon tomography facility based on large scale MRPC detectors. Nucl. Instrum. Methods A **784**, 390–393 (2015). https://doi.org/10.1016/j.nima.2015.01.024
11. L.J. Schultz, Dissertation, Portland State University (2003)
12. B. Yu, Z. Zhao, X. Wang et al., An MAP algorithm with edge-preserving prior for muon tomography, in IEEE Nuclear Science Symposium & Medical Imaging Conference. IEEE (2014). https://doi.org/10.1109/nssmic.2014.7431083